Inorg. Chem. **2008**, *47*, 1560−1567

Inorganic Chemistry
Article

A Tungsten(VI) Nitride Having a $W_2(\mu\text{-}N)_2$ Core

Zachary J. Tonzetich, Richard R. Schrock,* Keith M. Wampler, Brad C. Bailey, Christopher C. Cummins, and Peter Müller

Department of Chemistry 6-331, Massachusetts Institute of Technology, Cambridge, Massachusetts 02139

Received September 27, 2007

The tungsten nitrido species, $[W(\mu\text{-}N)(CH_2\text{-}t\text{-}Bu)(OAr)_2]_2$ (Ar = 2,6-diisopropylphenyl), has been prepared in a reaction between the alkylidyne species, $W(C\text{-}t\text{-}Bu)(CH_2\text{-}t\text{-}Bu)(OAr)_2$, and organonitriles. The dimeric nature of the nitride was established in the solid state through an X-ray study and in solution through a combination of ^{15}N NMR spectroscopy and vibrational spectroscopy. Reaction of the nitride with trimethylsilyl trifluoromethanesulfonate afforded the monomeric trimethylsilyl imido species, $W(NSiMe_3)(CH_2\text{-}t\text{-}Bu)(OAr)_2(OSO_2CF_3)$, which was also characterized crystallographically. The W_2N_2 core can be reduced by one electron electrochemically or in bulk with metallocenes to afford the radical anion, $\{n\text{-}Bu_4N\}\{[W(\mu\text{-}N)(CH_2\text{-}t\text{-}Bu)(OAr)_2]_2\}$. Density functional theory calculations suggest that the lowest-energy allowable transition in $[W(\mu\text{-}N)(CH_2\text{-}t\text{-}Bu)(OAr)_2]_2$ is from a highest occupied molecular orbital consisting largely of ligand-based lone pairs into what is largely a metal-based lowest unoccupied molecular orbital.

Introduction

Recently, we reported that the tungsten alkylidyne species $W(C\text{-}t\text{-}Bu)(CH_2\text{-}t\text{-}Bu)(OAr)_2$ (Ar = 2,6-diisopropylphenyl) can be prepared readily in a reaction between $W(OAr)_3Cl_3$ and four equivalents of $t\text{-}BuCH_2MgCl$.[1] In the process of exploring the chemistry of $W(C\text{-}t\text{-}Bu)(CH_2\text{-}t\text{-}Bu)(OAr)_2$, we observed that it reacts with nitriles to afford a pentane-soluble nitrido species, which we formulated as monomeric $W(N)(CH_2\text{-}t\text{-}Bu)(OAr)_2$ (eq 1) on the basis of the usual analytical techniques and its solubility in alkanes. The reaction of $W(C\text{-}t\text{-}Bu)(CH_2\text{-}t\text{-}Bu)(OAr)_2$ with nitriles was not unexpected, as similar reactions have been known since 1982.[2] Also, the *tris*-aryloxide nitride, $W(N)(OAr)_3$, is known to form upon the reaction of $W(C\text{-}t\text{-}Bu)(OAr)_3$ with acetonitrile at room temperature.[3]

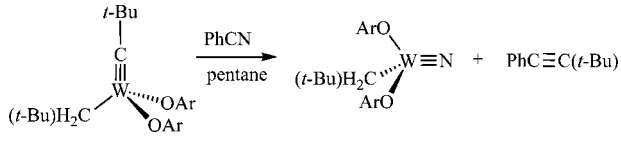

(1)

We became intrigued by the intense red color of $W(N)(CH_2\text{-}t\text{-}Bu)(OAr)_2$, which is unusual for a monomeric four-coordinate W(VI) nitride. Other structures of W(VI) nitrides such as linear polymers and cyclic trimers, formed through bonding of the nitride as a base *trans* to the nitride in the next metal-containing unit, have been identified with a variety of supporting ligands.[4] In no case were intense colors noted for these compounds. For example, the linear polymer, $[W(N)(O\text{-}t\text{-}Bu)_3]_\infty$, is colorless,[5] while the cyclic trimer, $\{W(N)[OCMe_2(CF_3)]_3\}_3$, is yellow.[6] $W(N)(OAr)_3$ is also relatively intensely colored and was shown to be a dimer in the solid state with a rare diamond-shaped $W_2(\mu\text{-}N)_2$ core.[4] Unfortunately, the insolubility of $[W(\mu\text{-}N)(OAr)_3]_2$ in common organic solvents prevented a detailed study of its structure in solution. Since $W(N)(CH_2\text{-}t\text{-}Bu)(OAr)_2$ is readily soluble in pentane, we were drawn to explore its structure in both the solid state and in solution in more detail. We report our findings here.

Results

A single crystal of $W(N)(CH_2\text{-}t\text{-}Bu)(OAr)_2$ was subjected to an X-ray diffraction study. Its structure is depicted in

* To whom correspondence should be addressed. E-mail: rrs@mit.edu.

(1) Tonzetich, Z. J.; Lam, Y. C.; Müller, P.; Schrock, R. R. *Organometallics* **2007**, *26*, 475.
(2) Schrock, R. R.; Listemann, M. L.; Sturgeoff, L. G. *J. Am. Chem. Soc.* **1982**, *104*, 4291.
(3) Freudenberger, J. H.; Schrock, R. R. *Organometallics* **1986**, *5*, 398.
(4) Pollagi, T. P.; Manna, J.; Geib, S. J.; Hopkins, M. D. *Inorg. Chim. Acta* **1996**, *243*, 177.
(5) Chisholm, M. H.; Hoffman, D. M.; Huffman, J. C. *Inorg. Chem.* **1983**, *22*, 2903.
(6) Chisholm, M. H.; Folting-Streib, K.; Tiedtke, D. B.; Lemoigno, F.; Eisenstein, O. *Angew. Chem., Int. Ed. Engl.* **1995**, *334*, 110.

10.1021/ic701913q CCC: $40.75
Published on Web 02/08/2008

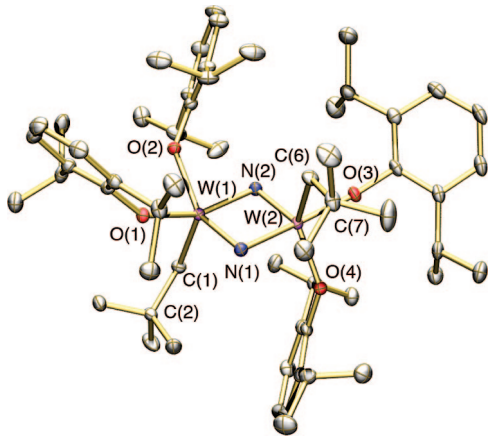

Figure 1. Thermal ellipsoid (50%) drawing of the structure of $[W(\mu\text{-}N)(CH_2\text{-}t\text{-}Bu)(OAr)_2]_2$. Selected bond distances (Å) and angles (deg): W(1)−C(1) = 2.111(2); W(1)−O(1) = 1.8952(15); W(1)−O(2) = 1.9567(15); W(2)−C(6) = 2.180(2); W(2)−O(3) = 1.9015(15); W(2)−O(4) = 1.9035(16); W(1)−C(1)−C(2) = 123.58(15); W(2)−C(6)−C(7) = 123.93(16). See Figure 2 for details within the W_2N_2 core.

Figure 1. Selected bond lengths and angles for the non-nitrido ligands are listed in the figure caption, and refinement parameters appear in Table 1. The compound is a dimer containing a $W_2(\mu\text{-}N)_2$ core similar to what is found for $[W(\mu\text{-}N)(OAr)_3]_2$.[4] The geometry about tungsten is best described as trigonal bipyramidal, with the nitrido ligands occupying one equatorial and one axial site. One aryloxide ligand occupies the other axial position, giving the molecule pseudoinversion symmetry. The bond distances and angles of the alkyl and aryloxide ligands are unexceptional and similar to those found for $[W(\mu\text{-}N)(OAr)_3]_2$.[4] The $W_2(\mu\text{-}N)_2$ core is planar, although not rigorously symmetric. The angles of the $W_2(\mu\text{-}N)_2$ core show small deviations from 90°, and the N−W−N angles are somewhat more acute (Figure 2). The W−N bonds show alternating short (av. 1.81 Å) and long (av. 1.95 Å) distances, with the shorter W−N bonds found in the equatorial positions of the trigonal bipyramids.

In order to elucidate the structure of $W(N)(CH_2\text{-}t\text{-}Bu)(OAr)_2$ in solution, we turned to ^{15}N NMR spectroscopy. The synthesis of $W(^{15}N)(CH_2\text{-}t\text{-}Bu)(OAr)_2$ was carried out employing $CH_3C^{15}N$ (eq 2).

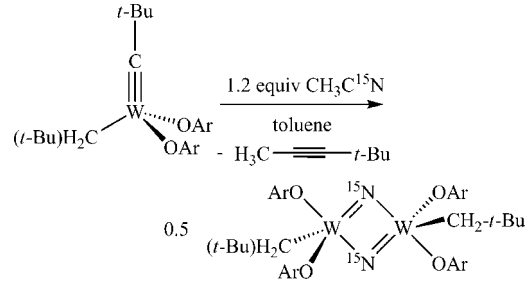

(2)

^1H and ^{13}C NMR spectra of $W(^{15}N)(CH_2\text{-}t\text{-}Bu)(OAr)_2$ are identical to those of $W(N)(CH_2\text{-}t\text{-}Bu)(OAr)_2$; no ^1H or ^{13}C atoms appear to be coupled to any significant degree to ^{15}N. The ^{15}N NMR spectrum displays a single peak at 680.3 ppm that has two sets of ^{183}W satellites (J_{WN} = 30.2 Hz; Figure 3). A monomeric structure would be expected to show one set of ^{183}W satellites with an area of ∼0.14 (∼0.07 per satellite) with respect to the total peak area. Two sets of ^{183}W

Table 1. Crystallographic and Refinement Details for $[W(\mu\text{-}N)(CH_2\text{-}t\text{-}Bu)(OAr)_2]_2$ and $W(^{15}NSiMe_3)(CH_2\text{-}t\text{-}Bu)(OAr)_2(OTf)$[a]

	$[W(\mu\text{-}N)(CH_2\text{-}t\text{-}Bu)(OAr)_2]_2$	$W(^{15}NSiMe_3)(CH_2\text{-}t\text{-}Bu)(OAr)_2(OTf)$
empirical formula	$C_{58}H_{90}N_2O_4W_2$	$C_{33}H_{54}F_3{}^{15}NO_5SSiW$
fw (g/mol)	1247.02	845.77
temp (K)	100(2)	218(2)
cryst syst	monoclinic	orthorhombic
space group	$P2_1/n$	$Pbca$
unit cell dimensions		
a	14.022(3) Å	18.9549(6) Å
b	18.198(3) Å	19.1661(6) Å
c	22.170(4) Å	21.8341(7) Å
α	90°	90°
β	92.105(3)°	90°
γ	90°	90°
vol (Å^3)	5653.4(18)	7932.1(4)
Z	4	8
density (calculated, g/cm^3)	1.465	1.416
absorption coefficient (mm^{-1})	4.110	3.045
F(000)	2528	3440
crystal size (mm^3)	0.15 × 0.15 × 0.10	0.35 × 0.20 × 0.20
θ range for data collection	1.83−29.57°	1.78−29.13°
index ranges	$-19 \le h \le +19$	$-25 \le h \le +25$
	$-25 \le k \le +25$	$-26 \le k \le +26$
	$-30 \le l \le +30$	$-29 \le l \le +29$
reflns collected	124692	166109
independent reflns	15860 [R(int) = 0.0514]	10671 [R(int) = 0.0423]
completeness to θ	100%	100%
max. and min. transmission	0.6840 and 0.5776	0.5811 and 0.4154
data/restraints/parameters	15860/5/629	10671/510/490
goodness-of-fit on F^2	1.032	1.069
final R indices [$I > 2\sigma(I)$]	R1 = 0.0210	R1 = 0.0235
	wR2 = 0.0465	wR2 = 0.0528
R indices (all data)	R1 = 0.0287	R1 = 0.0413
	wR2 = 0.0497	wR2 = 0.0630
largest diff. peak and hole (e Å^{-3})	2.899 and −1.041	0.710 and −0.797

[a] All diffraction data were collected using Mo Kα radiation (0.71073 Å). The absorption correction was semi-empirical from equivalents, and the refinement method was full-matrix least squares on F^2.

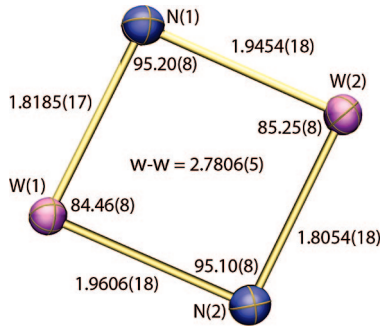

Figure 2. Relevant bond distances (Å) and angles (deg) within the W_2N_2 core of $[W(\mu\text{-}N)(CH_2\text{-}t\text{-}Bu)(OAr)_2]_2$.

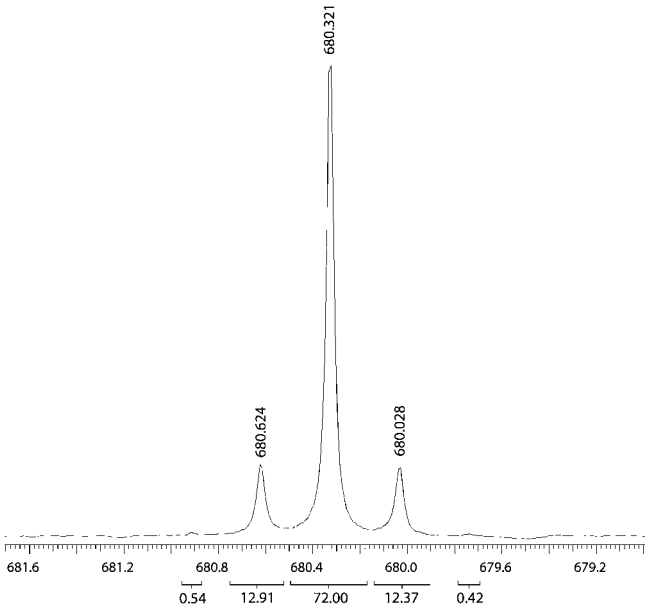

Figure 3. ^{15}N NMR (50.7 MHz) spectrum of $[W(\mu\text{-}N)(CH_2\text{-}t\text{-}Bu)(OAr)_2]_2$ in toluene-d_8 showing the areas of the ^{183}W satellites. Chemical shift values are in parts per million.

satellites are observed with approximate fractional areas of 0.26 and 0.02, a pattern that can only arise if ^{15}N (~100%) is approximately equally coupled to *two* ^{183}W nuclei. Coupling of ^{15}N to equivalent tungsten centers suggests that the molecule possesses higher symmetry in solution (on the NMR time scale) than found for the structure in the solid state. The methylene protons of the neopentyl ligand are also equivalent, consistent with the higher symmetry in solution. ^1H NMR spectra of the nitride at −70 °C in toluene-d_8 (see Figure 1S in the Supporting Information) are consistent with the slowing down of a fluxional process or processes and formation of a species of lower symmetry on the NMR time scale. We ascribe the symmetry observed in NMR spectra at 20 °C to a rapid intramolecular fluxional process within the dimeric species. This process is proposed to involve rearrangement about each five-coordinate metal core, a type of rearrangement that is often facile in high oxidation state species.

A dimeric structure that has an inversion center, as found for $[W(\mu\text{-}N)(CH_2\text{-}t\text{-}Bu)(OAr)_2]_2$ in the solid state, is expected to show three IR active normal modes of the $W_2(\mu\text{-}N)_2$ core (A_u symmetry in C_i). As shown in a partial infrared spectrum of the ^{14}N and ^{15}N isotopomers of $[W(\mu\text{-}N)(CH_2\text{-}t\text{-}Bu)(OAr)_2]_2$ in pentane (Figure 4), two peaks are observable at 836 and 651 cm^{-1} that shift in the ^{15}N-labeled species to 815 cm^{-1} ($\Delta = -21$ cm^{-1}) and 635 cm^{-1} ($\Delta = -16$ cm^{-1}). We assume that the third (out-of-plane mode) occurs at too low an energy to be observed in this experiment. The solution Raman spectrum of the nitride was also obtained, but no isotopically shifted peaks could be identified with certainty (see Figure 2S in the Supporting Information). The solution IR results are consistent with a dimeric structure in pentane solution.

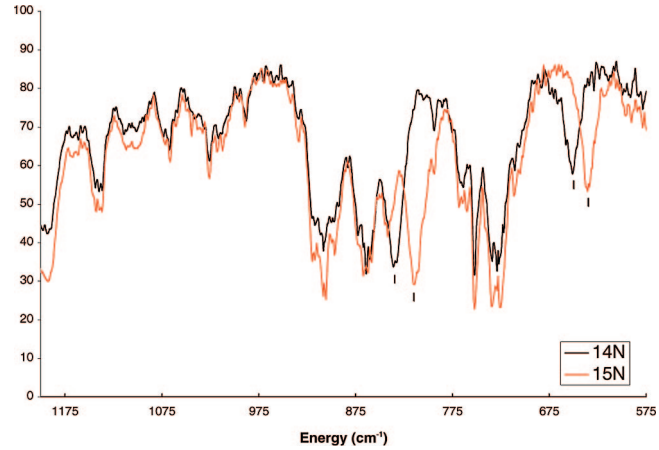

Figure 4. IR spectra of ^{14}N and ^{15}N isotopomers of $[W(\mu\text{-}N)(CH_2\text{-}t\text{-}Bu)(OAr)_2]_2$ in pentane (5.0 mM; KBr cell).

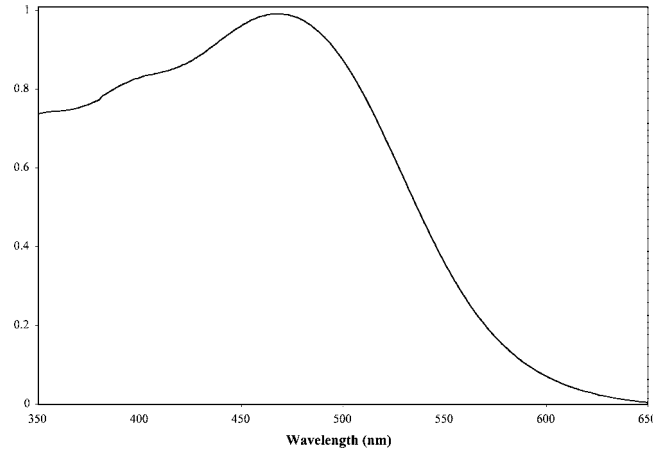

Figure 5. Electronic absorption spectrum of $[W(\mu\text{-}N)(CH_2\text{-}t\text{-}Bu)(OAr)_2]_2$ in pentane (λ_{max} = 480 nm; ϵ = 16 100 M^{-1} cm^{-1}).

The electronic absorption spectrum of $[W(\mu\text{-}N)(CH_2\text{-}t\text{-}Bu)(OAr)_2]_2$ in pentane is shown in Figure 5. A relatively intense broad absorption is centered at 480 nm with a higher energy shoulder near 400 nm. We will show in a later section devoted to density functional theory (DFT) calculations that the highest occupied molecular orbital (HOMO) consists largely of ligand-based lone pairs while the lowest unoccupied molecular orbital (LUMO) is largely a metal-centered orbital. Therefore, the intense absorption in $[W(\mu\text{-}N)(CH_2\text{-}t\text{-}Bu)(OAr)_2]_2$ is believed to arise from a HOMO → LUMO (ligand-to-metal charge transfer, LMCT) transition. The molar absorptivity (16 100 $M^{-1}cm^{-1}$) is actually twice what was reported in the preliminary communication,[1] since we had assumed at that stage that the nitride was a monomer.

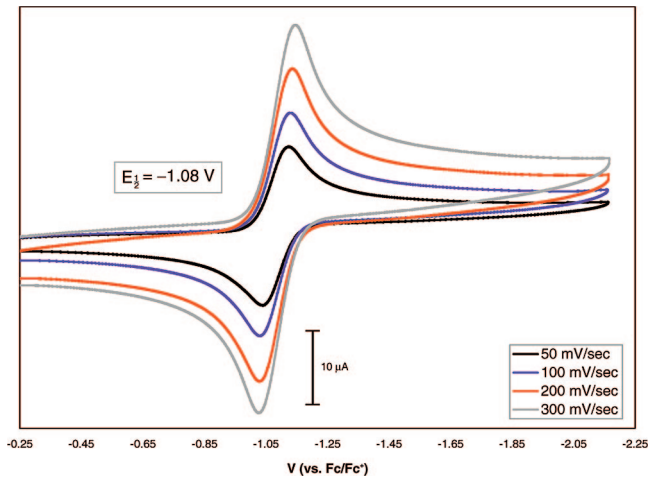

Figure 6. Cyclic voltamogram of $[W(\mu\text{-}N)(CH_2\text{-}t\text{-}Bu)(OAr)_2]_2$ in THF (2.0 mM). Conditions: 0.4 M n-Bu_4NPF_6, glassy carbon electrode, 2.4 mM Cp_2Fe internal standard.

The precise nature of the LCMT is covered in more detail in a later section.

The cyclic voltamogram of $[W(\mu\text{-}N)(CH_2\text{-}t\text{-}Bu)(OAr)_2]_2$ in THF (Figure 6) reveals a reversible 0/- couple at −1.08 V versus Fc/Fc^+. No other redox couples could be identified in the CV within the solvent window (THF). Chemical reduction of $[W(\mu\text{-}N)(CH_2\text{-}t\text{-}Bu)(OAr)_2]_2$ was accomplished with Cp_2Co in THF. Subsequent addition of n-Bu_4NPF_6 afforded the radical anion as the TBA salt (eq 3), which crystallizes as black needles from diethyl ether.

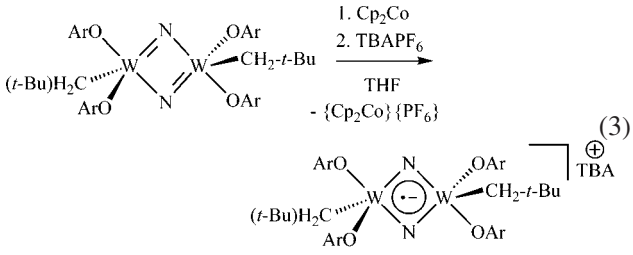

(3)

A proton NMR spectrum of the radical anion shows several broadened peaks (See Figure 3S in the Supporting Information), although the chemical shift range remains relatively small (∼12 ppm), consistent with an unpaired electron that remains largely within the $W_2(\mu\text{-}N)_2$ core. The addition of AgOTf to the radical anion salt in THF-d_8 immediately affords $[W(\mu\text{-}N)(CH_2\text{-}t\text{-}Bu)(OAr)_2]_2$(eq 4).

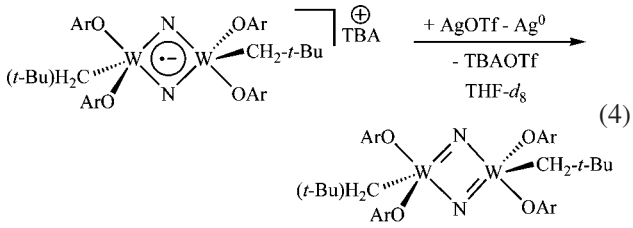

(4)

In IR spectra of $\{n\text{-}Bu_4N\}\{[W(\mu\text{-}N)(CH_2\text{-}t\text{-}Bu)(OAr)_2]_2\}$ and $\{n\text{-}Bu_4N\}\{[W(\mu\text{-}^{15}N)(CH_2\text{-}t\text{-}Bu)(OAr)_2]_2\}$, only one absorption could be clearly identified as a W−N vibration (at 507 cm^{-1} in the former and 492 cm^{-1} in the latter). These values should be compared with those at 836 and 651 cm^{-1}

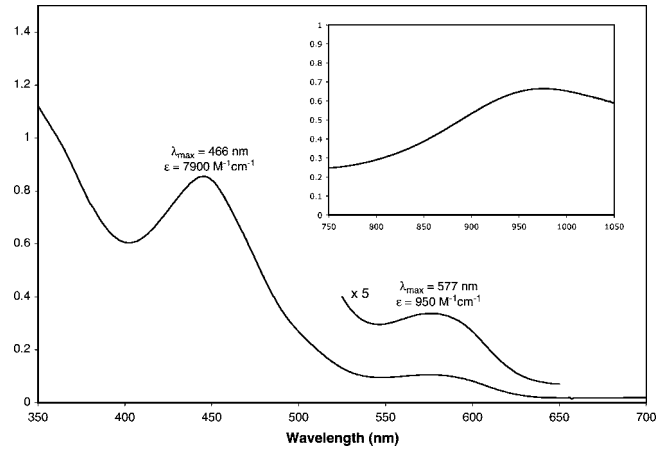

Figure 7. Electronic absorption spectrum of $\{n\text{-}Bu_4N\}\{[W(\mu\text{-}N)(CH_2\text{-}t\text{-}Bu)(OAr)_2]_2\}$ in diethyl ether.

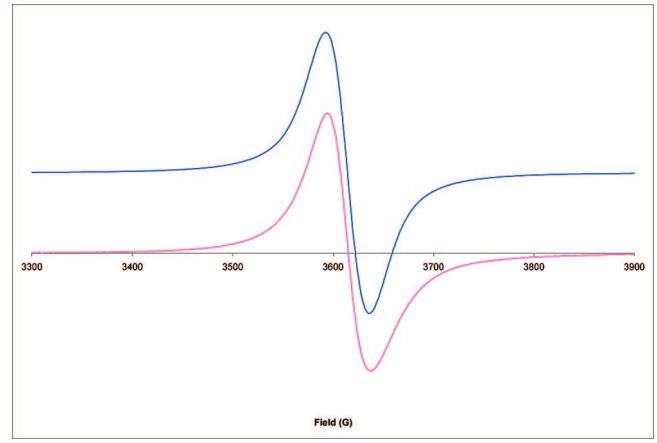

Figure 8. Experimental (bottom) and simulated (top) EPR spectra for $\{n\text{-}Bu_4N\}\{W(\mu\text{-}^{14}N)(CH_2\text{-}t\text{-}Bu)(OAr)_2]_2\}$ at 293 K: g_{iso} = 1.913 and W_{iso} = 43 G.

for $[W(\mu\text{-}N)(CH_2\text{-}t\text{-}Bu)(OAr)_2]_2$ and $[W(\mu\text{-}^{15}N)(CH_2\text{-}t\text{-}Bu)(OAr)_2]_2$, respectively. The 507 cm^{-1} absorption is at considerably lower energy than either 836 or 651 cm^{-1} and would suggest that the bonding within the $W_2(\mu\text{-}N)_2$ core of the anion is significantly weaker, consistent with addition of the electron to a $W_2(\mu\text{-}N)_2$ orbital that has substantial metal character.

The electronic absorption spectrum of $\{n\text{-}Bu_4N\}\{[W(\mu\text{-}N)(CH_2\text{-}t\text{-}Bu)(OAr)_2]_2\}$ in diethyl ether (Figure 7) displays an intense absorption at 466 nm, similar to what is found in the neutral nitride, but at slightly lower energy and with about half the intensity. A less intense band (ϵ = 950 M^{-1} cm^{-1}) is also observed at 577 nm. A third absorption is observed at 978 nm with an even lower intensity (ϵ = 570 M^{-1} cm^{-1}).

The experimental and simulated electron paramagnetic resonance (EPR) spectra for $\{n\text{-}Bu_4N\}\{[W(\mu\text{-}N)(CH_2\text{-}t\text{-}Bu)(OAr)_2]_2\}$ at room temperature can be found in Figure 8. An essentially identical spectrum is observed for $\{n\text{-}Bu_4N\}\{[W(\mu\text{-}^{15}N)(CH_2\text{-}t\text{-}Bu)(OAr)_2]_2\}$ except g_{iso} = 1.918 and W_{iso} = 70 G. The experimental and simulated EPR spectra for $\{n\text{-}Bu_4N\}\{[W(\mu\text{-}^{14}N)(CH_2\text{-}t\text{-}Bu)(OAr)_2]_2\}$ at 77 K are shown in Figure 9, while the analogous spectra for $\{n\text{-}Bu_4N\}\{[W(\mu\text{-}^{15}N)(CH_2\text{-}t\text{-}Bu)(OAr)_2]_2\}$ are shown in Figure 10. Coupling to both ^{15}N (100%) and ^{183}W (15%)

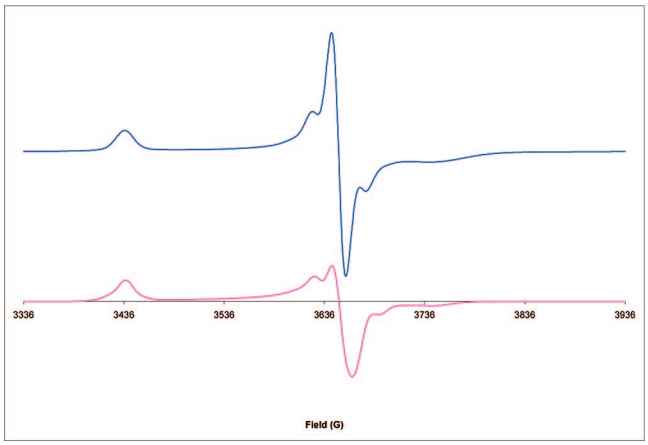

Figure 9. Experimental (bottom) and simulated (top) EPR spectra for {*n*-Bu4N}{[W(μ-^{14}N) (CH_2-*t*-Bu)($OAr)_2]_2$} at 77 K. $g_x = 2.012$, $g_y = 1.894$, $g_z = 1.841$, $W_x = 17$ G, $W_y = 9$ G, $W_z = 65$ G, and A_y ($2\ ^{183}$W, $I = 1/2$, 14.31%) = 44 G.

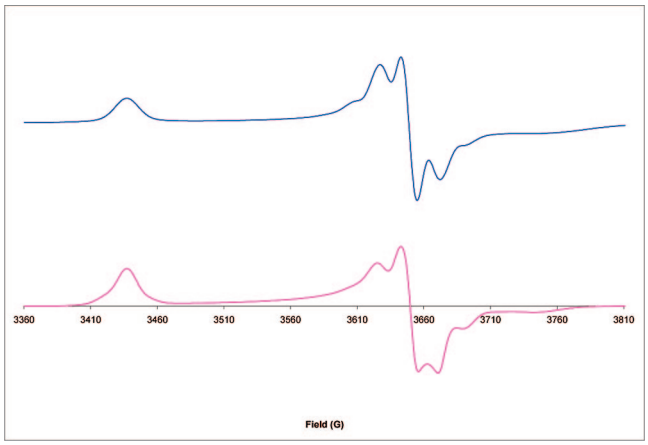

Figure 10. Experimental (bottom) and simulated (top) EPR spectra for {*n*-Bu_4N}{[W(μ-^{15}N)(CH_2-*t*-Bu)($OAr)_2]_2$} at 77 K. $g_x = 2.012$, $g_y = 1.894$, $g_z = 1.841$, $W_x = 17$ G, $W_y = 9$ G, $W_z = 63$ G, A_y ($2\ ^{183}$W, $I = 1/2$, 14.31%) = 44 G, A_y ($2\ ^{15}$N, $I = 1/2$, 100%) = 16 G.

suggests that the semioccupied molecular orbital in the anion has some density on both W and N.

The nitride reacts cleanly with TMSOTf in pentane over a period of 2 days at 23 °C to give the trimethylsilylimido species shown in eq 5. The imido complex can be isolated as brilliant red needles from pentane. ^{1}H NMR spectra are consistent with the structure drawn in eq 5. The methylene protons of the alkyl ligand appear as a singlet resonance at 2.58 ppm ($J_{HW} = 10.5$ Hz) in benzene-d_6. The ^{15}N NMR spectrum of the ^{15}N isotopomer displays a single resonance at 453.6 ppm. The single set of satellites ($J_{NW} = 103$ Hz) is consistent with coupling to one ^{183}W nucleus. (See Figure 4S in the Supporting Information). This larger coupling constant is indicative of a monomeric imido structure in solution and should be compared to a coupling constant of 30.2 Hz in the nitride. IR spectra of W($NSiMe_3$)(CH_2-*t*-Bu)($OAr)_2$(OTf) in pentane show a peak at 1146 cm^{-1} that shifts to 1120 cm^{-1} in W($^{15}NSiMe_3$)(CH_2-*t*-Bu)($OAr)_2$(OTf). This vibrational mode cannot be assigned unambiguously as the W=N stretch, since in transition metal imido complexes the W=N stretch can couple with the N−X stretch (where X is Si in this case); [7] elucidation of this vibrational mode therefore would require further experiments.

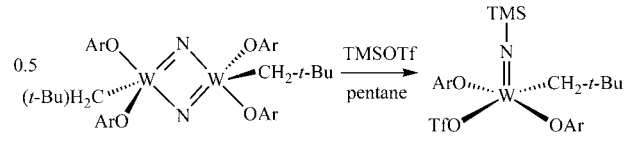

(5)

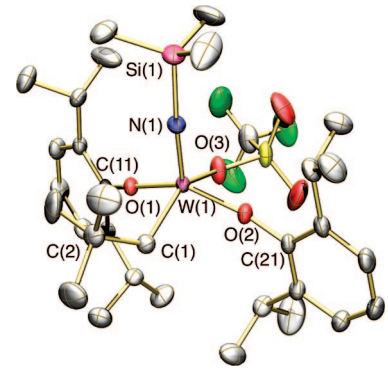

Figure 11. Thermal ellipsoid (30%) drawing of the structure of W($NSiMe_3$)(CH_2-*t*-Bu)($OAr)_2$(OTf). Selected bond distances (Å) and angles (deg): W(1)−N(1) = 1.718(2); W(1)−C(1) = 2.146(3); W(1)−O(1) = 1.8428(17); W(1)−O(2) = 1.8425(17); W(1)−O(3) = 2.147(2); N(1)−Si(1) = 1.774(2); O(1)−W(1)−O(2) = 146.43(8); C(1)−W(1)−O(3) = 147.02(11); C(1)−W(1)−N(1) = 102.09(11); O(1)−W(1)−O(3) = 78.82(8); C(1)−W(2)−O(2) = 88.00(10); W(1)−N(1)−Si(1) = 170.25(16); W(1)−C(1)−C(2) = 126.1(2).

The structure of the trimethylsilylimide complex was confirmed through an X-ray diffraction study of W($^{15}NSiMe_3$)-(CH_2-*t*-Bu)($OAr)_2$(OTf) (Figure 11). Due to a destructive phase change in the crystal near −60 °C, diffraction data had to be collected at −55 °C. Consequently, the triflate ligand was disordered, and the thermal motion of the atoms was greater than normal (thermal ellipsoids shown in Figure 11 at 30%). Metric data for the complex are listed in the caption and refinement details can be found in Table 1. The structure is essentially a square pyramid, with nearly identical bond angles about the equatorial plane. The W(1)−N(1) distance of 1.718(2) Å is significantly shorter than the corresponding W−N contacts in the nitride species. The W−O−C_{ipso} bonds of the 2,6-diisopropylphenoxide ligands are quite obtuse (average = 166.9°), demonstrating the sterically congested nature of this five-coordinate compound.

DFT calculations on [W(μ-N)(CH_2-*t*-Bu)($OAr)_2]_2$ were carried out with the Amsterdam Density Functional (ADF) package.[8] No truncation approximations were made; that is, the molecule was employed in its entirety as the initial computational model. The functional selected to augment the local exchange-correlation potential of Vosko et al.[9] (VWN) was the nonhybrid BP86 functional (see Becke[10] and

(7) Osborne, J. H.; Trogler, W. C. *Inorg. Chem.* **1985**, *24*, 3098.
(8) (a) te Velde, G.; Bickelhaupt, F. M.; Baerends, E. J.; Fonseca Guerra, C.; van Gisbergen, S. J. A.; Snijders, J. G.; Ziegler, T. *J. Comput. Chem.* **2001**, *22*, 931. (b) Baerends, E. J. *ADF, ADF2006.01*; Theoretical Chemistry, Vrije Universiteit: Amsterdam, The Netherlands, **2004**. http://www.scm.com (accessed Dec 2007). (c) Fonseca Guerra, C.; Snijders, J. G.; te Velde, G.; Baerends, E. J. *Theor. Chem. Acc.* **1998**, *99*, 391.
(9) Vosko, S. H.; Wilk, L.; Nusair, M. *Can. J. Phys.* **1980**, *58*, 1200.
(10) Becke, A. D. *Phys. Rev. A: At., Mol., Opt. Phys.* **1988**, *38*, 3098.

Perdew[11]), as this has been seen to give excellent results for geometries and energies when applied to organometallic systems.[12] In order to expedite the calculations, large basis sets were employed only for the core atoms (W, N, O, and the two C atoms bonded directly to W; these atoms were treated using a TZ2P basis as supplied by ADF), while for all the peripheral C and H atoms, a small basis set of DZ quality was utilized. In order to speed up the computation, the system was subjected to geometry optimization using the C_i point group symmetry, even though the molecule exhibited only C_1 symmetry in the solid state, as determined by X-ray crystallography. The initial model used in the geometry optimization was derived from half of the dimeric structure obtained in the X-ray study. Given the presence of heavy W atoms, it was important to include relativistic effects, and this was done accordingly using the ZORA method.[13] It was observed that the computationally optimized structure was a close mimic of the structure determined by experimentation, in terms of the core interatomic distances and angles.

The 10 lowest-energy allowed excitations were calculated using the time-dependent density functional response equations incorporated in the ADF program.[14] Of all the allowed excitations, that with the lowest energy (2.0076 eV, 618 nm) was found to be dominated by electron promotion from HOMO to LUMO. This same transition was also found to be the one, of those calculated, with the greatest oscillator strength ($f = 0.16727$ au). For this reason, our discussion of the UV/vis spectrum of the μ-nitrido dimer is limited to this particular transition.

In order to understand the nature of this transition, we consider the atomic orbital composition of the HOMO and the LUMO. The HOMO is characterized by an even distribution of lone-pair orbitals from the atoms directly bonded to tungsten, except for the neopentyl groups, where the metal–carbon σ-bonding electrons contribute (Figure 12). No tungsten orbital contributes to the HOMO to any significant degree. In contrast, the LUMO gains its greatest contribution from tungsten d-orbital functions, while it also can be seen (Figure 12) to have W−O π^* character in addition to a small amount of W−N bonding character. In this respect, the low-energy transition may be interpreted as a LMCT transition. This is similar to the case analyzed by Tuczek et al.,[15] with the difference being that the observed low-energy transition (530 nm; calculated at 500 nm) was assigned as a HOMO-1 → LUMO excitation, but still one that has a LMCT origin.

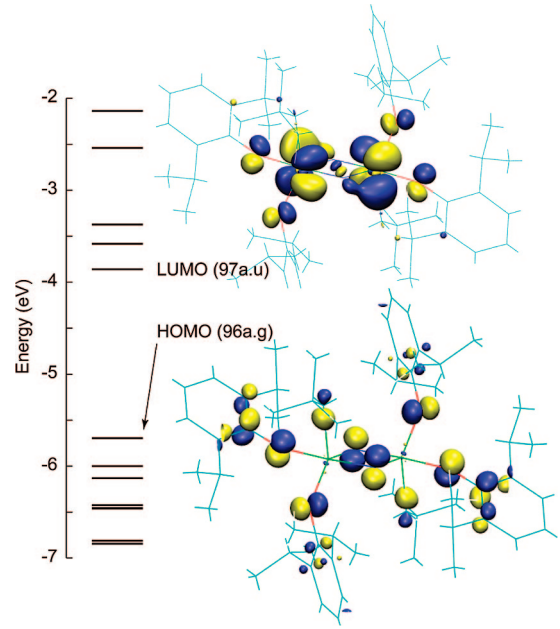

Figure 12. Energy level diagram calculated for the neutral μ-nitrido dimer, together with graphical depictions of the HOMO and LUMO at the 95% probability level.

Discussion and Conclusions

Nitrido complexes of d^0 metals form a variety of structures that vary from monomers to cyclic oligomers (trimers and tetramers especially) to polymers.[16] $M_2(\mu\text{-}N)_2$ cores where M is in its highest possible oxidation state are rare. The first structurally characterized example, $[(\eta^5\text{-}C_5Me_5)V(\mu\text{-}N)Cl_2]_2$, was reported by Doherty et al.,[17] while other vanadium examples were published later by Cloke et al.[18] and Heberhold et al.[19] Examples of the $M_2(\mu\text{-}N)_2$ core with the heavier group V metals have been published recently by Sita et al.[20] (Ta) and Floriani et al. (Nb).[21] Structurally characterized examples of non-d^0 $M_2(\mu\text{-}N)_2$ compounds include an anionic vanadium species[22] and a dimeric chromium(V) nitride.[23] Interest in several of these $M_2(\mu\text{-}N)_2$ species stems largely from their formation from molecular nitrogen.[18,20] An example is the formation of a d^0 $Ta_2(\mu\text{-}N)_2$ species from a Ta(IV)(μ-N_2)Ta(IV) species [if the μ-N_2 fragment is viewed as $(\mu\text{-}N_2)^{4-}$]. In this compound, the two electrons required for N−N bond cleavage come from the two Ta(IV) centers. The reason why dimers are formed from monomeric d^0 metal nitrides in a few cases (instead of trimers, tetramers, etc.) is not understood, although a subtle balance of steric factors

(11) (a) Perdew, J. P. *Phys. Rev. B: Condens. Matter Mater. Phys.* **1986**, *33*, 8822. (b) Perdew, J. P. *Phys. Rev. B: Condens. Matter Mater. Phys.* **1986**, *34*, 7406.
(12) Deng, L. Q.; Schmid, R.; Ziegler, T. *Organometallics* **2000**, *19*, 3069.
(13) (a) van Lenthe, E.; Baerends, E. J.; Snijders, J. G. *J. Chem. Phys.* **1993**, *99*, 4597. (b) van Lenthe, E.; Baerends, E.; Snijders, J. *J. Chem. Phys.* **1994**, *101*, 9783. (c) van Lenthe, E.; Ehlers, A.; Baerends, E. *J. Chem. Phys.* **1999**, *110*, 8943.
(14) van Gisbergen, S. J. A.; Snijders, J. G.; Baerends, E. J. *Comput. Phys. Commun.* **1999**, *118*, 119.
(15) Studt, F.; Lamarche, V. M. E.; Clentsmith, G. K. B.; Cloke, F. G. N.; Tuczek, F. *Dalton Trans.* **2005**, 1052.
(16) (a) Schoeller, W. W.; Sundermann, A. *Inorg. Chem.* **1998**, *37*, 3034. (b) Dehnicke, K.; Strähle, J. *Angew. Chem., Int. Ed. Engl.* **1992**, *31*, 955.
(17) Haddad, T. S.; Aistars, A.; Ziller, J. W.; Doherty, N. M. *Organometallics* **1993**, *12*, 2420.
(18) (a) Clentsmith, G. K. B.; Bates, V. M. E.; Hitchcock, P. B.; Cloke, F. G. N. *J. Am. Chem. Soc.* **1999**, *121*, 10444. (b) Bates, V. M. E.; Clentsmith, G. K. B.; Cloke, F. G.N.; Green, J. C.; Jenkin, H. D. L. *Chem. Commun.* **2000**, 927.
(19) Herberhold, M.; Dietel, A.-M.; Goller, A.; Milius, W. *Z. Anorg. Allg. Chem.* **2003**, *629*, 871.
(20) Hirotsu, M.; Fontaine, P. P.; Epshteyn, A.; Zavalij, P. Y.; Sita, L. R *J. Am. Chem. Soc.* **2007**, *129*, 9284.
(21) Caselli, A.; Solari, E.; Scopelliti, R.; Floriani, C.; Re, N.; Rizzoli, C.; Chiesi-Villa, A. *J. Am. Chem. Soc.* **2000**, *122*, 3652.
(22) Berno, P.; Gambarotta, S. *Angew.Chem., Int. Ed.* **1995**, *34*, 822.
(23) Odom, A. L.; Cummins, C. C. *Organometallics* **1996**, *15*, 898.

clearly will play an important role.

The compounds closest to those we have discussed here are the vanadium compounds $[(L)V(\mu\text{-}N)]_2$ and $K\{[(L)V(\mu\text{-}N)]_2\}$, where L is the dianionic diamido/donor ligand, $[Me_3SiN(CH_2CH_2NSiMe_3)_2]^{2-}$.[18] X-ray structural studies of both have been carried out, as have studies of their formation and a study of the vibrational and electronic structure of $[(L)V_2(\mu\text{-}N)]_2$.[15] A potassium cation is bound to a nitride nitrogen in $K\{[(L)V(\mu\text{-}N)]_2\}$, as one might expect in the absence of a ligand that could sequester the ion. In the IR study of $[(L)V_2(\mu\text{-}N)]_2$, two absorptions at 798 cm^{-1} (788 cm^{-1} in the ^{15}N species) and 656 cm^{-1} (643 cm^{-1} in the ^{15}N species) were identified and assigned to the two asymmetric in-plane V−N vibrations. Although these absorptions are not resolved as clearly in the vanadium system (Figure 4 in ref 15) as in the tungsten system studied here, they are in remarkable agreement with the absorptions found at 836 cm^{-1} (815 cm^{-1} in the ^{15}N species) and 651 cm^{-1} (635 cm^{-1} in the ^{15}N species) in the tungsten system studied here. One might have expected the difference in energy of the vibrations to be greater because of the low mass of V compared to W. The two electronic absorptions found in the $[(L)V_2(\mu\text{-}N)]_2$ system at 530 and 400 nm (weak) should be compared with the 480 and 400 nm (weak) absorptions observed in the tungsten system. The HOMO → LUMO transition in $[(L)V_2(\mu\text{-}N)]_2$ was calculated to occur at 570 nm and to have no intensity. Therefore, the authors concluded that the transition occurs from the HOMO-1 to the LUMO where the HOMO-1 has amido nitrogen lone pair character and the LUMO has a 70% vanadium d orbital contribution, that is, a LMCT (amido lone pair to metal). The calculations that we have carried out on the tungsten system suggest that the HOMO → LUMO transition is allowed and is also a LMCT.

Experimental Section

General. All manipulations were performed in oven-dried (200 °C) glassware under an atmosphere of nitrogen on a dual-manifold Schlenk line or in a Vacuum Atmosphere glovebox. High-performance liquid chromatography grade organic solvents were sparged with nitrogen and dried by passage through activated alumina, then stored over 4 Å Linde-type molecular sieves prior to use. Benzene-d_6 was dried over sodium/benzophenone ketyl and vacuum-distilled prior to use, then stored over 4 Å Linde-type sieves. NMR spectra were recorded in benzene-d_6 on a Varian Mercury or Varian INOVA spectrometer operating at 300 or 500 MHz (^1H), respectively. Chemical shifts for ^1H and ^{13}C spectra were referenced to the residual $^1H/^{13}C$ resonances of the solvent (^1H, δ 7.16; ^{13}C, δ 128.39) and are reported as parts per million relative to tetramethylsilane. Reported coupling constants are for H−H couplings unless otherwise noted. Elemental analyses were performed by H. Kolbe Microanalytics Laboratory, Mülheim an der Ruhr, Germany.

Solution magnetic moments were determined at 298 K in THF-d_8 with hexamethyldisiloxane as the internal standard according to the Evans method.[24] EPR spectra were recorded on an X-band Bruker EMX spectrometer. WINEPR SimFonia (*WINEPR SimFonia*, version 1.25; Bruker Analytische Messtechnik GmbH, Karlsruhe, Germany, 1996.) was employed to simulate the spectra. For low-temperature EPR simulations, a linear combination of an anisotropic simulation and an isotropic simulation was employed in order to account for coupling to both tungsten and nitrogen.

$[W(\mu\text{-}N)(CH_2\text{-}t\text{-}Bu)(OAr)_2]_2$. A flask was charged with 0.2494 g (0.368 mmol) of W(C-*t*-Bu)(CH_2-*t*-Bu)$(OAr)_2$ and 15 mL of pentane. To the yellow solution was added 45 μL (0.44 mmol) of benzonitrile. The solution was allowed to stir at room temperature for 2 days during which time it became dark red. All volatiles were removed *in vacuo*, and the residue was dissolved in 3 mL of pentane. The solution was set aside at −25 °C for 24 h, yielding 0.1808 g (79%) of iridescent black crystals that were isolated by decantation of the mother liquor. ^1H NMR (300 MHz): δ 7.09 (d, 8, *m*-Ar), 6.95 (t, 4, *p*-Ar), 3.53 (sep, 8, C*H*Me_2), 2.86 (s, 4, CH_2, J_{HW} = 10.5 Hz), 1.24 (d, 24, CH*Me*$_2$), 1.20 (d, 24, CH*Me*$_2$), 1.12 (s, 18, *t*-Bu). ^{13}C NMR (125 MHz): δ 157.1, 140.0, 124.8, 124.3, 77.1 (*C*H_2-*t*-Bu, J_{CW} = 104 Hz), 36.4, 34.4, 28.1, 24.6. IR (KBr, pentane): cm^{-1} 1326, 1252, 1193, 836 (WN), 752, 651 (WN). Anal. Calcd for $C_{29}H_{45}NO_2W$: C, 55.86; H, 7.27; N, 2.25. Found: C, 56.08; H, 7.36; N, 2.27.

$[W(\mu\text{-}^{15}N)(CH_2\text{-}t\text{-}Bu)(OAr)_2]_2$. Prepared in identical fashion as above from $CH_3C^{15}N$ in toluene. ^{15}N NMR (50.7 MHz, toluene-d_8): δ 680.3 (J_{NW} = 30.2 Hz). IR (KBr, pentane): cm^{-1} 815 (WN), 635 (WN).

{*n*-Bu_4N}{$[W(\mu\text{-}N)(CH_2\text{-}t\text{-}Bu)(OAr)_2]_2$}. A flask was charged with 192.2 mg (0.154 mmol) of $\{[W(CH_2\text{-}t\text{-}Bu)(OAr)_2]_2\text{-}m_2\text{-}(N)_2\}$ and 5 mL of THF. The solution was cooled to −25 °C, at which point 30.5 mg (0.161 mmol) of $CoCp_2$ was added as a solution in 2 mL of THF. The reaction was stirred at room temperarure for 30 min, during which time the color changed from dark red to brown-yellow. To the reaction solution was added 62.5 mg (0.161 mmol) of $TBAPF_6$ as a solution in 3 mL of THF, causing precipitation of a bright yellow precipitate. The mixture was set aside at −25 °C for 1 h to ensure complete precipitation. The mixture was filtered through celite, and all the volatiles were removed *in vacuo*. The resulting brown residue was crystallized from diethyl ether at −25 °C to yield 102 mg (45%) of black-brown needles that were washed with pentane and dried *in vacuo*. ^1H NMR (300 MHz, THF-d_8): δ 10.6 ($\nu_{1/2}$ = 189 Hz), 9.7, 3.2 ($\nu_{1/2}$ = 23 Hz), 1.9 ($\nu_{1/2}$ = 170 Hz), 1.7 ($\nu_{1/2}$ = 41 Hz), 1.4 (TBA), 1.3 (TBA), 1.2, 1.1 (TBA), 1.0, 0.9 (TBA). μ_{eff} (THF-d_8, 298 K) = 2.30 μ_B. IR (KBr, THF): cm^{-1} 1586, 1332, 748, 575, 507 (WN). Anal. Calcd for $C_{74}H_{126}N_3O_4W_2$: C, 59.67; H, 8.53; N, 2.82. Found: C, 59.43; H, 8.65; N, 2.74.

{*n*-Bu_4N}{$[W(\mu\text{-}^{15}N)(CH_2\text{-}t\text{-}Bu)(OAr)_2]_2$}. This compound was prepared from $[W(\mu\text{-}^{15}N)(CH_2\text{-}t\text{-}Bu)(OAr)_2]_2$ in an identical fashion to that described for $\{n\text{-}Bu_4N\}\{[W(\mu\text{-}N)(CH_2\text{-}t\text{-}Bu)(OAr)_2]_2\}$. ^1H NMR (300 MHz, THF-d_8): δ 10.6 (fwhm = 189 Hz), 9.7, 3.2 (TBA), 1.9, 1.7, 1.4 (TBA), 1.3 (TBA), 1.1 (TBA). IR (KBr, THF) cm^{-1} 1586, 1332, 748, 575, 492 (WN).

$W(NSiMe_3)(CH_2\text{-}t\text{-}Bu)(OAr)_2(OTf)$. A flask was charged with 0.106 g (0.169 mmol) of $\{[W(CH_2\text{-}t\text{-}Bu)(OAr)_2]_2\text{-}\mu_2\text{-}(N)_2\}$ and 8 mL of pentane. To the stirring solution was added 35 μL (0.18 mmol) of TMSOTf via syringe. The solution was allowed to stir at room temperature for 45 h, during which time the color lightened from dark red to bright red. All volatiles were removed *in vacuo*, and the residue was dissolved in 2 mL of pentane. The solution was set aside at −25 °C for 24 h, yielding 0.0983 g (80%) of bright red needles in two crops. ^1H NMR (300 MHz): δ 7.06 (d, 4, *m*-Ar), 6.94 (t, 2, *p*-Ar), 3.65 (sep, 4, C*H*Me_2), 2.58 (s, CH_2, J_{HW} = 10.2 Hz), 1.36 (app t, 24, CH*Me*$_2$), 0.97 (s, 9, *t*-Bu), 0.39 (s, 9, Si*Me*$_3$). ^{13}C NMR (125 MHz): δ 159.0 (*ipso*-Ar), 140.4 (*o*-Ar), 127.1 (*p*-Ar), 124.5 (*m*-Ar), 120.8 (q, J_{CF} = 319 Hz, *C*F_3), 83.1 (*C*H_2, J_{CW} = 126 Hz), 36.3 (*C*Me_3), 33.8, 28.0, 25.1, 24.3, 2.0 (Si*Me*$_3$). ^{19}F

(24) (a) Evans, D. F. *J. Chem. Soc.* **1959**, 2003. (b) Schubert, E. M. *J. Chem. Educ.* **1992**, *69*, 62. (c) Grant, D. H. *J. Chem. Educ.* **1995**, *72*, 39.

NMR (282 MHz): δ −77.2 (OSO_2CF_3). IR (KBr, pentane): 1252, 1236, 1199, 1146, 1101, 969, 919, 906, 845, 635. Anal. Calcd for $C_{33}H_{54}F_3NO_5SSiW$: C, 46.86; H, 6.44; N, 1.66. Found: C, 46.34; H, 6.40; N, 1.58.

$W(^{15}NSiMe_3)(CH_2\text{-}t\text{-}Bu)(OAr)_2(OTf)$. This compound was prepared from $[W(\mu\text{-}^{15}N)(CH_2\text{-}t\text{-}Bu)(OAr)_2]_2$ in an identical manner to that described for $W(NSiMe_3)(CH_2\text{-}t\text{-}Bu)(OAr)_2(OTf)$. ^{15}N NMR (50.7 MHz): δ 453.6 (J_{NW} = 103 Hz). IR (KBr, pentane): cm^{-1} 1120.

Acknowledgment. R.R.S. (CHE-0138495) and C.C.C (CHE-0719157) thank the National Science Foundation for supporting this research. We thank Dr. Timothy McClure in the Center for Materials Science and Engineering (CMSE) for help in obtaining Raman spectra.

Supporting Information Available: Fully labeled thermal ellipsoid drawings (Figures 1S−4S) and crystallographic information files in cif format. This material is available free of charge via the Internet at http://pubs.acs.org. X-ray crystallographic data for $[W(\mu\text{-}N)(CH_2\text{-}t\text{-}Bu)(OAr)_2]_2$ (07014) and $W(^{15}NSiMe_3)(CH_2\text{-}t\text{-}Bu)(OAr)_2(OTf)$ (07030) are also available to the public at http://reciprocal.mit.edu.

IC701913Q